Reducing Velocity Uncertainty with a Deblurring Filter

Shihang Feng[1], Oz Yilmaz[2,3], Yuqing Chen[1] and Sherif Hanafy[1]
[1]King Abdullah University of Science and Technology (KAUST), Division of Physical Science and Engineering, Thuwal, Saudi Arabia
[2]Anatolian Geophysical
[3]GeoTomo LLC

ABSTRACT

We present a workflow for constructing a zero-offset reflection section that preserves most of the reflections and diffractions. This workflow includes the construction of a migration image volume by prestack time migration using a series of constant velocity models. A deblurring filter for each constant velocity model is applied to each time-migration image to get a deblurred image volume. In order to preserve all events in the image volume, each image panel is demigrated and then summed over the velocity axis. The resulting demigration section is equivalent to a zero-offset reflection section. Numerical tests are used to validate the advantages and limitations of this method.

INTRODUCTION

Normal moveout (NMO) velocity analysis using semblance is an important step in building an initial subsurface velocity model (**?**). Conventional velocity analysis methods of seismic gathers scan different values of effective moveout velocity, compute the semblance of flattened gathers and generate velocity spectra for later velocity picking (**?**). However, the NMO correction doesn't provide optimal focusing of reflection energy for dipping reflectors since NMO does not acount for lateral movement of migrated reflection event. This problem is usually overcome with the help of dip moveout (DMO) (**??**). As an alternative, time migration velocity analysis takes into account both vertical and lateral movements of migrated reflection events. (**???**).

In areas with a structurally complex subsurface, the semblance spectrum may have several peaks that give rise to uncertainties in velocity picking. These uncertainties are ignored by choosing certain peaks in the semblance spectrum. Then seismic images are structurally distorted because of the inevitable errors in velocity estimation (**?**). Understanding and quantifying the uncertainties in geophysical information can be important for seismic exploration (**?**). **?** studied the influence of velocity uncertainties on migrated images and AVO attribues. **?** related velocity picking uncertainties and structural sensitivity with structural uncertainties.

It is difficult to account for the velocity uncertainties since they are a combination of various factors, such as lateral velocity variations, heterogeneity and anisotropy. Instead of eliminating these uncertainties, a workflow is designed to get velocity independent zero-offset gathers and therefore circumvent the velocity uncertainty problem (**??**). Here we incorporate a deblurring filter into this workflow to improve the quality of the composite zero-offset reflection section.

After the introduction, the next section summarizes the theory of this method, and the workflow is in the third section. Numerical tests on synthetic and field data are shown in the next section and the conclusions are in the last section.

THEORY

Deblurring Filter

Linearized forward modeling of seismic data can be represented by applying the linear modeling operator $\mathbf{L}$ to the reflectivity model $\mathbf{m}$ to get the forward modeled data $\mathbf{d}$,

$$\mathbf{d} = \mathbf{L}\mathbf{m}. \quad (1)$$

The migration image $\mathbf{m}_{mig}$ is computed by applying the migration operator $\mathbf{L^T}$ to the observed data,

$$\mathbf{m}_{mig} = \mathbf{L^T d} = \mathbf{L^T L m}, \tag{2}$$

where $\mathbf{L^T L}$ is the blurring operator (**?**). In addition, equation **??** can be written as

$$\mathbf{m} = (\mathbf{L^T L})^{-1}\mathbf{m}_{mig}. \tag{3}$$

where the migration image $\mathbf{m}_{mig}$ is the blurred representation of the actual reflectivity model $\mathbf{m}$. **?** showed $\mathbf{m}_{mig}$ can be deblurred by a good estimate of $(\mathbf{L^T L})^{-1}$.

The direct computation of the inverse of the Hessian operator $\mathbf{L^T L}$ is too expensive. But it will be cheaper to calculate an approximation of the inverse Hessian. To approximate the inverse Hessian, deblurring operators are designed and used as a preconditioning operator (**????**).

For the deblurring operator used by **?** and **?**, a grid model with an even distribution of isolated point scatterers $\mathbf{m}_{ref}$ is used as the reference model. Then we have

$$\mathbf{m}_{mig\_ref} = \mathbf{L^T L m}_{ref} = \mathbf{L^T d}_{ref}, \tag{4}$$

where $\mathbf{L}$ only depends the background velocity and the source-receiver configurations (**?**). The images $\mathbf{m}_{ref}$ and $\mathbf{m}_{mig\_ref}$ are divided into subsections centered around each point scatterer. In each subsection, a deblurring filter is estimated by locally matching the point-scatterer model with the migration image $m_{mig_{ref}}$ as

$$[\mathbf{m}_{ref}]_i = [\mathbf{m}_{mig\_ref}]_i \star \mathbf{f}_i, \tag{5}$$

where i indicates the ith subsection, $[\quad]_i$ denotes the model in the $i$the subsection and $\star$ is a convolution operator.

Equation **??** can be rewritten in matrix notation

$$\mathbf{m}_{ref} = \mathbf{F m}_{mig\_ref}. \tag{6}$$

Since $\mathbf{m}_{ref}$ is an approximation of $\mathbf{m}$, $\mathbf{F}$ is the approximated preconditioner matrix

$$\mathbf{F} \approx (\mathbf{L}^T\mathbf{L})^{-1}. \tag{7}$$

Further details for computing $\mathbf{F}$ are given in **?** and **?**.

Construction of the Zero-offset Wavefield

For a constant velocity model, the sequence of NMO, DMO, CMP stack, and poststack migration operations are kinematically equivalent to prestack migration (**???**). Following **???**. This statement can be expressed by the following equation:

$$NMO + DMO + stack + tmig = PSTM. \tag{8}$$

where *tmig* stands for time migration after stack. **??** utilized this equivalence to construct the zero-offset wavefield as described by equation 9. Add *demig* to both sides of equation 8 to get:

$$\begin{aligned} &NMO + DMO + stack + tmig + demig \\ &= PSTM + demig. \end{aligned} \tag{9}$$

where *demig* stands for demigration — in this case, *inverse of tmig*. This means that the terms *tmig* and *demig* on the left-side of the equation cancel each other, and we obtain:

$$NMO + DMO + stack = PSTM + demig, \tag{10}$$

Note that the left-side of this equation yields the $zero-offset\ wavefield$:

$$zero-offset\ wavefield = PSTM + demig. \tag{11}$$

To improve the signal-to-noise ratio, **??** applied a multichannel Cadzow filter based on eigenimage decomposition (**?**) to the velocity panels of the migration cube created by PSTM prior to demigration of each velocity panel. Alternatively, in this paper, we modify equation 9, by adding *deblur* to both sides of this equation to get:

$$\begin{aligned} &NMO + DMO + stack + tmig + deblur + demig \\ &= PSTM + deblur + demig. \end{aligned} \tag{12}$$

On the left side, the application of *tmig*+*deblur*+*demig* to the data can be represented by

$$\mathbf{LFL}^T\mathbf{d} \approx \mathbf{L}(\mathbf{L}^T\mathbf{L})^{-1}\mathbf{L}^T\mathbf{d}, \tag{13}$$

Then we have

$$zero-offset\ wavefield = PSTM + deblur + demig. \tag{14}$$

This equation says that the zero-offset reflection section can be constructed by the demigration of the deblurred PSTM images.

WORKFLOW

To circumvent velocity uncertainty, the following workflow shown in Figure **??** is presented in 6 steps, where the goal is to get a zero-offset reflection section without committing to a velocity model.

(1) Perform prestack time migration on all the shot gathers using a series of constant velocity models. The set of images form an image volume in (V, X, T) coordinates, where V is the rms velocity, X is the midpoint, and T is the event time.

(2) Build a reference grid model in (V, X, T) coordinates as illustrated in Figure **??**a. Simulate the reference data using Born modeling with the same constant velocity model used for PSTM in step 1.

(3) Apply prestack time migration to the reference data using the same series of constant velocity models. The set of migration image panels form a reference volume in the (V, X, T) coordinates.

(4) Use the reference volume and the reference model to calculate the deblurring filter for each constant velocity model as in Figure **??**. Then apply these deblurring filters to each migration image to get a series of deblurred migration panels and form a deblurred migration cube.

(5) Demigrate each of the deblurred migration panels employing the same constant velocity model used for PSTM in step 1 to create a zero-offset volume in the (V, X, T) coordinates.

(6) Apply a Radon transform to each of the velocity gathers in the (V, T) panels to reduce the horizontal smearing of amplitudes.

(7) Sum over the velocity axis to obtain a composite zero-offset reflection section that preserves all of the reflections and diffractions.

SYNTHETIC TESTS

Point Scatterer Model

The point scatterer model in Figure **??** is used to test this methodology, where the model size is 2.5 km in the X direction and 1.6 km in the Z direction with a grid spacing of 6.25 m. 25 sources are located on the surface with a spacing of 100 m. The data are recorded by 400 receivers spaced with an interval of 6.25 m and the source wavelet is a Ricker wavelet with a peak frequency of 15 Hz.

The zero-offset section obtained from the synthetic data is shown in Figure **??**a. For comparison, the composite zero-offset sections with and without deblurring are shown in Figures **??**b and **??**c, where the deblurring filter balances the energy of the zero-offset section. In Figure **??**, the traces at $x = 1.25\ km$ in these three zero-offset sections are compared and shows that the trace of the composite zero-offset section without deblurring suffers from wavelet stretch. The deblurring filter compensates for the wavelet stretch and the corresponding trace is consistent with that from the original data.

Overthrust Model

The overthrust model is shown in Figure **??**, where the model size is 4 km in the X direction and 1.6 km in the Z direction with a grid spacing of 10 m. One hundred sources are located on the surface with a spacing of 40 m, and the vertical-component traces are recorded by 400 receivers spaced with an interval of 10 m on the surface. The source wavelet is a Ricker wavelet with a peak frequency of 15 Hz.

The top rows of Figure **??** compare the true and composite zero-offset sections before and after deblurring.. The deblurred zero-offset reflection section has fewer artifacts and greater similarity with the true zero-offset section than the section without filtering. The zoom view of the sections are shown in the bottom row of Figure **??**.

GOM Data

The proposed methods are tested on a 2D marine data set. There are 100 shots with a shot interval of 37.5 m, and each shot is recorded by a 6 km long cable with 480 receivers spaced with a 12.5 m receiver interval. The receiver offset from the source is 200 m and the data are processed by a 25-Hz Wiener filter (**?**). Here the source wavelet is extracted from the raw data by stacking the time-shifted reflection events together from 200 to 250 m offset in the shot gather. The reflection traveltimes are then used to shift the traces so the reflection events from the same interface are flattened. These flattened reflection events are stacked together to get an estimate of the source wavelet.

The common offset gather shown in Figure **??**a at $x = 200\ m$ is regarded as a pseudo zero-offset section. The composite zero-offset sections with and without deblurring in Figure **??**b and **??**c contains all the reflections and diffractions in the pseudo zero-offset section. The deblurring filter increases the resolution of the reflection events at 4 s around $x = 1\ km$.

An example of the time migration images with a constant velocity equal to 1.6 km/s before and after deblurring are shown in Figure **??**. In the left side, it compensates for poor illumination and increases the resolution of the image.

First-arrival traveltime tomography is used to compute the v_{p0} model in Figure **??**a, where the first-arrivals only provide the low-intermediate wavenumber information in the shallow part of the model. Consequently, the tomogram has velocity errors in the deeper parts of the model. Thus, deep the reflection events in the prestack image will be mispositioned, defocused and even missing. The Kirchhoff prestack migration image and its zoom view are shown in Figures **??**b and Figure **??**b, respectively. In the area where the red arrows point, we can clearly see that the events are missing. The composite zero-offset data without and with deblurring are migrated by Kirchhoff poststack migration, where the images and their zoom views are shown in Figures **??**c, **??**d, **??**c and **??**d, respectively. The reflection events deblurred composite zero-offset data are slightly more continuous than the image without deblurring.

CONCLUSION

In the near surface areas with complex structures, there are can be significant velocity uncertainties in the RMS velocity estimate. To reduce these uncertainties, apply a deblurring filter to reconstruct a composite zero-offset reflection section that does not commit to a specified velocity model. The proposed workflow provides a composite zero-offset that contains most of the reflection and diffractions. In the synthetic and field tests, the composite zero-offset wavefield with a deblurring has better quality than the one without a deblurring. The composite zero-offset wavefield can then be migrated by poststack time

migration.

ACKNOWLEDGEMENTS

The research reported in this publication was supported by the King Abdullah University of Science and Technology (KAUST) in Thuwal, Saudi Arabia. We are grateful to the sponsors of the Center for Subsurface Imaging and Modeling Consortium for their financial support. For computer time, this research used the resources of the Supercomputing Laboratory at KAUST and the IT Research Computing Group. We thank them for providing the computational resources required for carrying out this work.

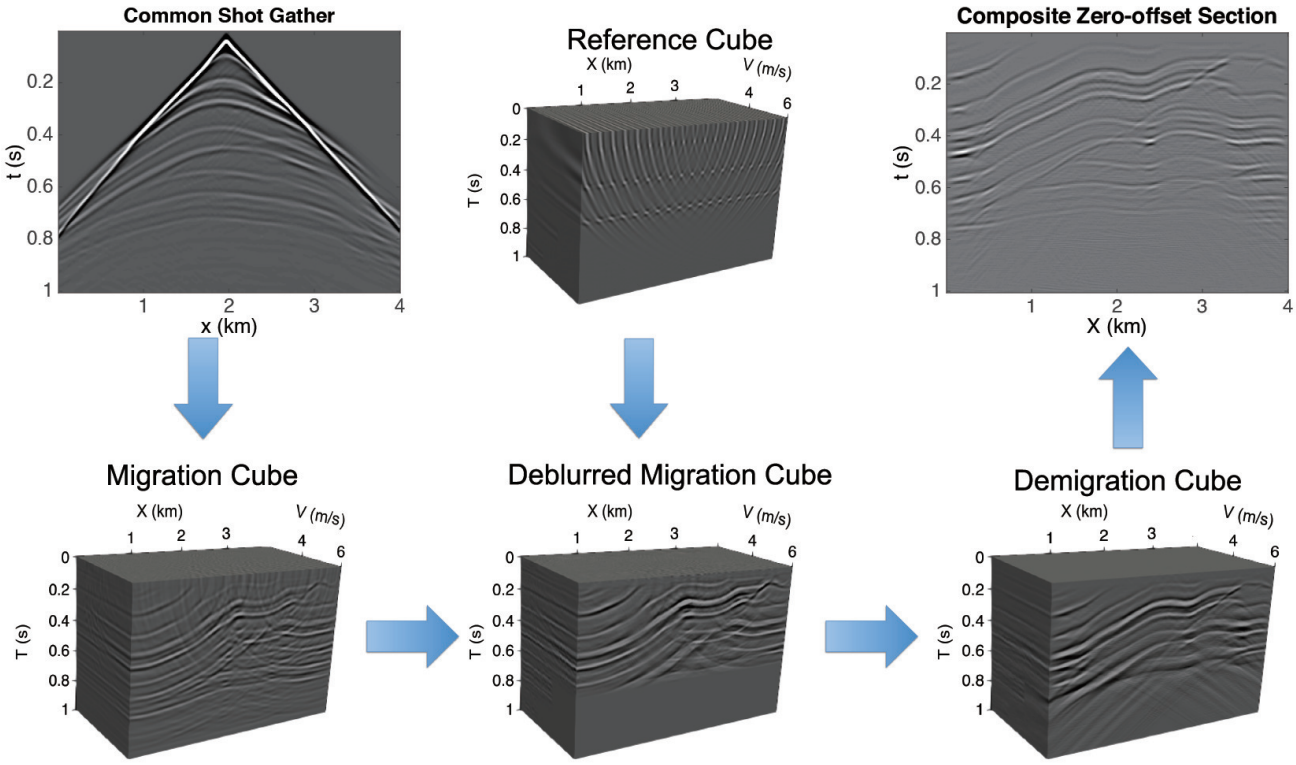

Figure 1: The workflow for constructing a zero-offset reflection section.

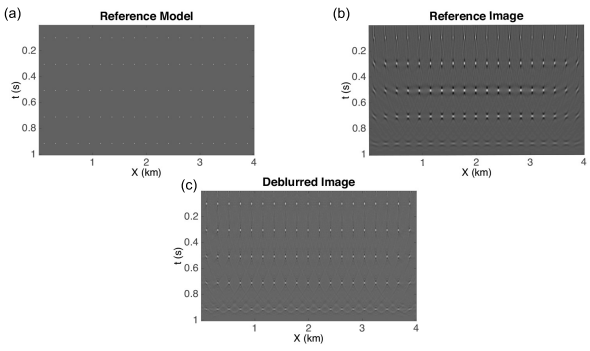

Figure 2: a) The reference reflectivity model containing isolated point diffractors, b) the corresponding time-migration image and c) the deblurred migration image.

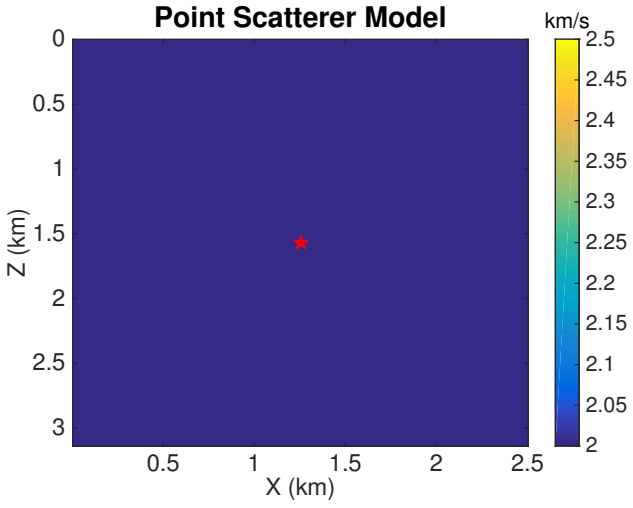

Figure 3: The point scatterer model.

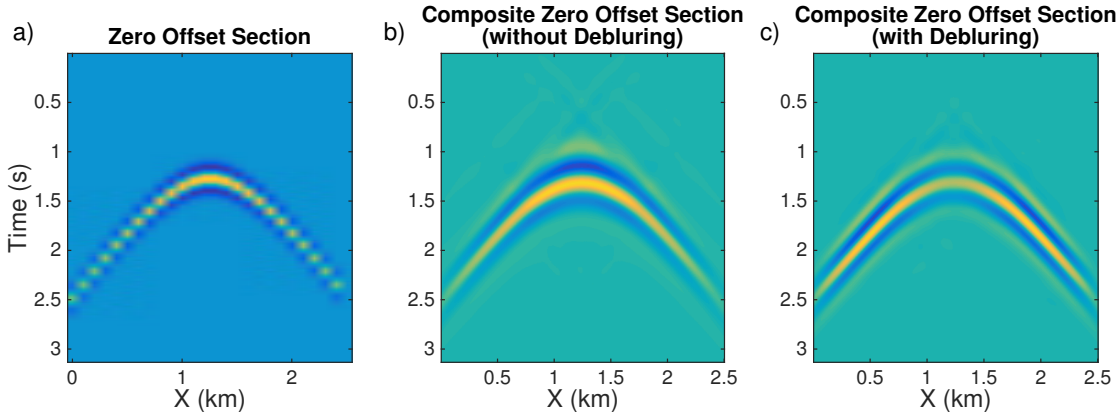

Figure 4: a) The zero-offset reflection section, the composite zero-offset sections b) without and c) with deblurring for the point-scatterer model.

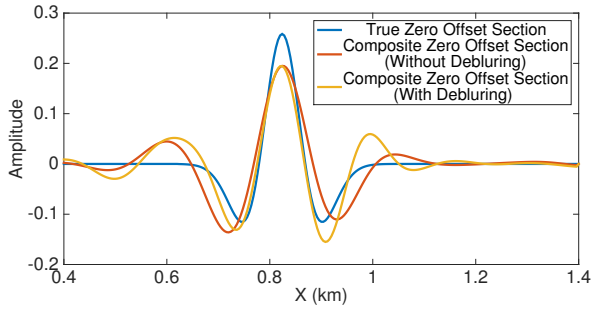

Figure 5: The traces at x=1.25 km from the true (blue), composite with (yellow) and without (red) deblurring zero-offset sections for the point-scatterer model.

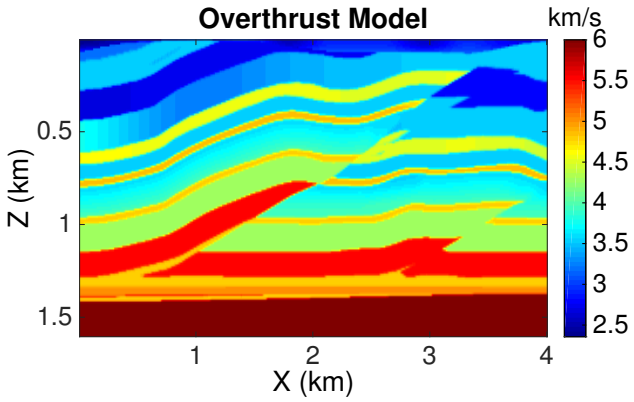

Figure 6: The overthrust model.

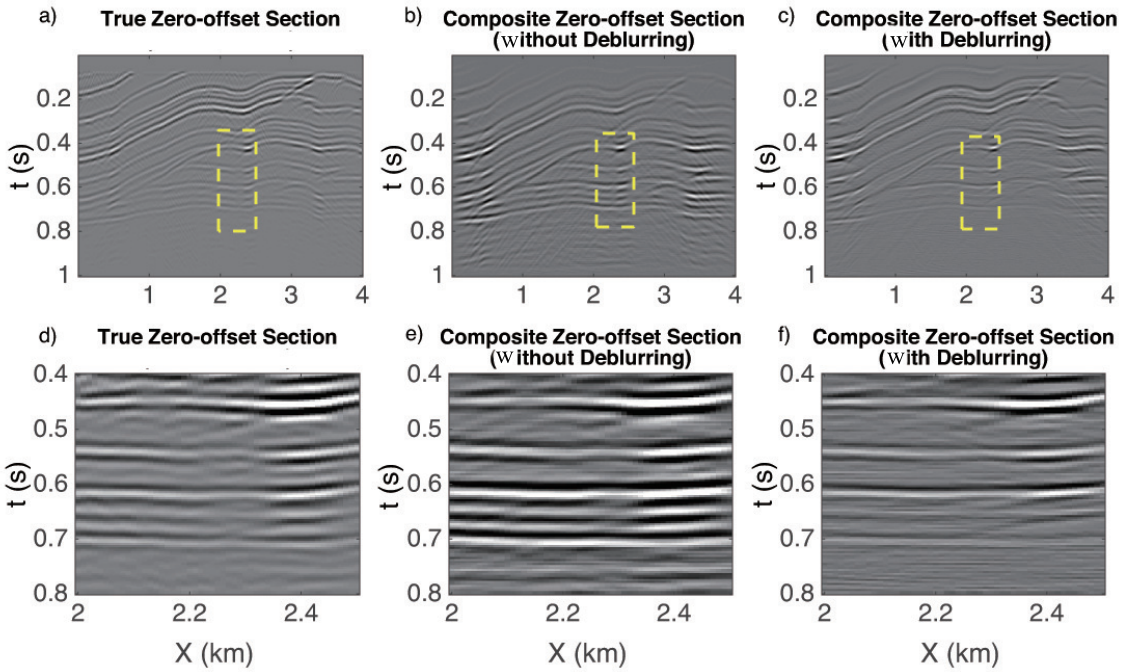

Figure 7: Top row: The zero-offset reflection sections obtained from a) the observed shot gathers, summation of the demigration panels b) without and c) with deblurring using overthrust data. The bottom row: Zoom views of the yellow boxes.

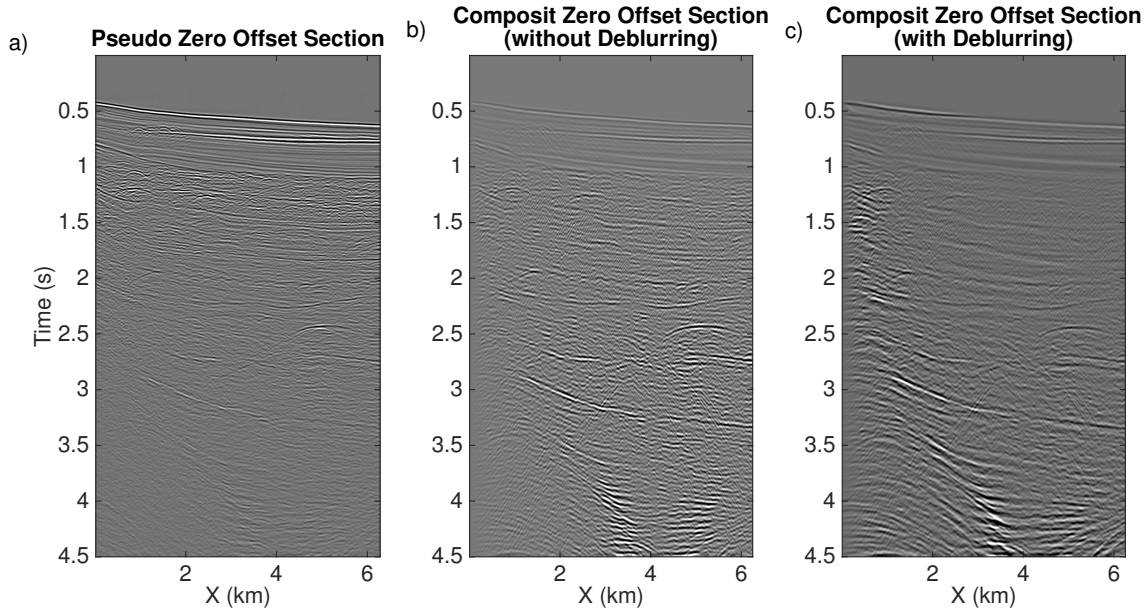

Figure 8: a) The pesudo zero-offset reflection section, the composite zero-offset section b) without and c) with deblurring for the GOM data.

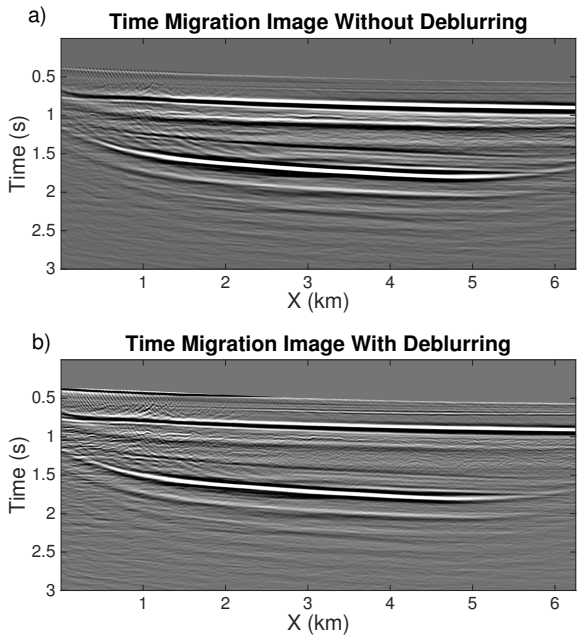

Figure 9: The time-migration image a) without and b) with the deblurring.

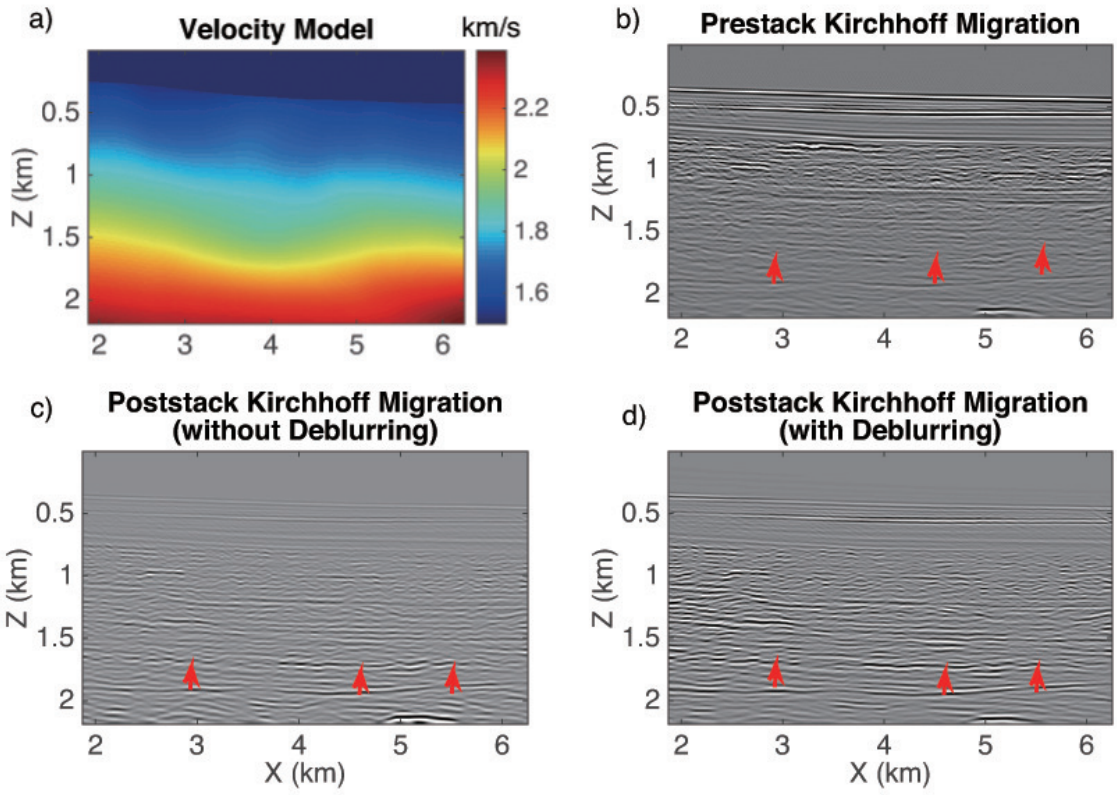

Figure 10: a) The migration velocity model and the images from b) the prestack Kirchhoff migration , the poststack Kirchhoff migration using composite zero-offset data b) without and c) with deblurring using the GOM data.

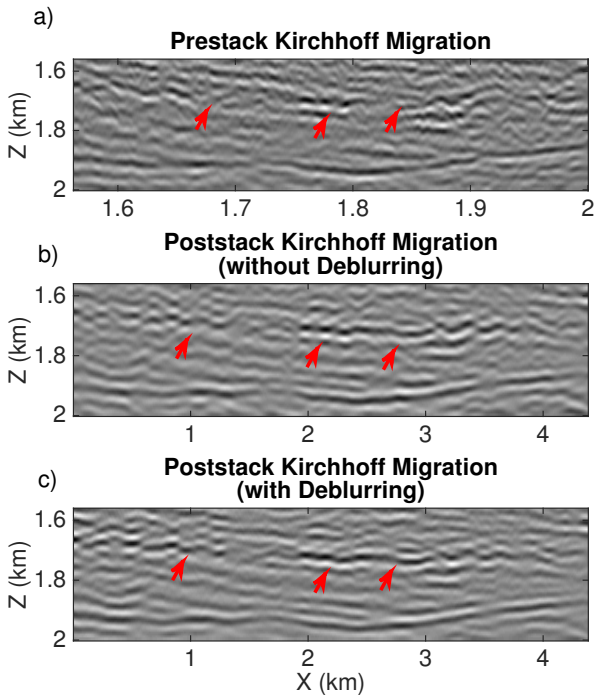

Figure 11: Zoom views of the Figure 10 migration images from the a) prestack Kirchhoff migration and b) poststack Kirchhoff migration.